atmosphere

MDPI

Article

A Comparison of Einstein *A* Coefficients for OH Rotational Temperature Measurements Using a Large Astronomical Data Set

Murdock Hart

Department of Astronomy, Boston University, 725 Commonwealth Ave, Boston, MA 02215, USA; murdock@bu.edu

Received: 10 July 2019; Accepted: 20 September 2019; Published: 22 September 2019

Abstract: The Einstein *A* coefficients are considered to be a significant source of uncertainty in the measurement of OH rotational temperatures. Using simultaneous ground and spaced-based observations of OH emission, five sets of Einstein *A* coefficients were examined for their impact upon rotational temperature calculations. The ground-based observations are taken from the Apache Point Observatory Galactic Evolution Experiment (APOGEE) instrument which is a high resolution, $r = \lambda/\Delta\lambda \geq 20,000$, spectrograph operating in the H-band from approximately 1.5 to 1.7 μm. APOGEE collected over one-hundred-and-fifty-thousand spectra of the night sky over a period from June 2011 to June 2013. The Sounding of the Atmosphere using Broadband Emission Radiometry (SABER) instrument on board the Thermosphere Ionosphere Mesosphere Energetics and Dynamics (TIMED) satellite has made simultaneous atmospheric measurements with the APOGEE spectrograph. SABER observes the OH volume emission rate (VER) around 1.6 μm, providing measurements coincident with those of the OH emission in the APOGEE sky spectra. Four of the five sets of Einstein *A* coefficients tested yielded statistically identical mean rotational temperatures of approximately 195 K for the OH$(4-2)$ transition. The Einstein *A* coefficients were found to have a significant impact upon the measured OH$(v' = 4)$ vibrational populations with some sets of coefficients yielding populations over 50% greater. Simultaneous SABER observations were used to determine which set of Einstein *A* coefficients best reflected atmospheric temperatures, and four of the five tested coefficients yielded nearly identical results. The difference between OH rotational temperatures and SABER temperatures was on average 1 K.

Keywords: OH; airglow; mesopause; rotational temperature; SDSS; APOGEE; TIMED; SABER

1. Introduction

The measurement of OH rotational temperatures is used as a proxy for atmospheric temperatures near the mesopause, but significant problems exist in their measurement. von Savigny et al. [1] demonstrated that the altitude of peak OH emission varied with vibrational level, and Cosby and Slanger [2], Noll et al. [3], and Hart [4] all showed that measured OH rotational temperatures were strongly dependent upon the upper vibrational level. Pendleton et al. [5], Cosby and Slanger [2], and Noll et al. [3] all found significant deviations from local thermal equilibrium (LTE) for the higher OH rotational levels, which artificially increase measured rotational temperatures. The Einstein *A* coefficients are another source of uncertainty in the measurement of OH rotational temperatures, and numerous researchers, such as Mies [6], Langhoff et al. [7], Turnbull and Lowe [8], Goldman et al. [9], Cosby and Slanger [2], and Liu et al. [10], have attempted to identify the transition probabilities which best reflect observations.

Mies [6] used the theoretical dipole moment of Stevens et al. [11] to derive transition probabilities, and in a comparison with available data found discrepancies in prior rotational temperature

measurements. Langhoff et al. [7] also used a theoretical electronic dipole moment function (EDMF) to derive the transition probabilities for the electronic ground state of the OH molecule. By comparing the average ratio of Einstein A coefficients, Langhoff et al. [7] determined that their theoretical transition probabilities better matched observations than the transition probabilities of Mies [6].

Turnbull and Lowe [8] used an empirical EDMF to calculate the electronic ground state transition probabilities of the OH molecule. To test the validity of their transition probabilities, they calculated the population of a single vibrational level using multiple overtones as this technique should yield the same population for all overtones. Turnbull and Lowe [8] found the transition probabilities of Mies [6] and Langhoff et al. [7] both failed this test, and determined that their transition probabilities derived consistent populations for a single upper vibrational level using multiple overtones.

Nelson et al. [12] used the relative intensities of 88 pairs of transitions of the OH electronic ground state to measure the OH dipole moment. These relative intensities provided detailed information about the shape of the OH EDMF, and the transition probabilities. Goldman et al. [9] used the improved line positions of Abrams et al. [13] and Melen et al. [14], along with the EDMFs of Nelson et al. [12] and Chackerian et al. [15], to determine the electronic ground state OH line parameters for a larger range of rotational states. van der Loo and Groenenboom [16] derived a new EDMF for OH in the ground electronic state based upon high-level ab initio calculations. They primarily found good agreement with the EDMF of Nelson [12], except at large atomic separations, where the EDMF of Nelson [12] decreased too fast. Using their EDMF, van der Loo and Groenenboom [16] calculated new transition probabilities for the OH molecule.

Cosby and Slanger [2] employed the method of Turnbull and Lowe [8] to find the transition probabilities that best matched the sky spectra collected by astronomical instruments, and found the transition probabilities of Goldman et al. [9] best matched their observations. Liu et al. [10] calculated the $\mathrm{OH}(9-4)$, $\mathrm{OH}(8-3)$, $\mathrm{OH}(6-2)$, $\mathrm{OH}(5-1)$, and $\mathrm{OH}(3-0)$ rotational temperatures using the transition probabilities from Mies [6], Turnbull and Lowe [8], Rothman et al. [17], van der Loo and Groenenboom [16], and Langhoff [7]. These rotational temperatures were compared to the Sounding of the Atmosphere using Broadband Emission Radiometry (SABER) volume emission rate (VER) profile weighted temperatures to determine which set of Einstein A coefficients best matched the observations. Liu et al. [10] determined that the coefficients of Langhoff [7] were the most consistent with the SABER data.

In this paper, we use the large number of sky spectra in the Apache Point Observatory Galactic Evolution Experiment (APOGEE) dataset to examine the effect that the Einstein A coefficients have upon ground-based OH rotational temperature measurements. The Einstein A coefficients used in this paper were taken from Mies [6], Turnbull and Lowe [8], Rothman et al. [17], van der Loo and Groenenboom [16], and Langhoff [7]. Column density calculations were also made using the five sets of Einstein A coefficients, and the effect they have upon column density measurements was examined. The APOGEE measured OH rotational temperatures were compared to the simultaneous SABER satellite-based observations, in an attempt to determine which set of Einstein A coefficients best reflected physical conditions. Both APOGEE and SABER observe emission from the $\mathrm{OH}(4-2)$ transition minimizing systematic errors due to the stratification of the OH vibrational levels, and were observed concurrently to minimize seasonal differences. Four of the five sets of Einstein A coefficients tested yielded nearly identical mean rotational temperatures, but the Einstein A coefficients were found to have a significant impact upon the measured $\mathrm{OH}(\mathrm{v}'=4)$ vibrational populations.

This manuscript is divided into eight sections. The introduction concludes here in Section 1. Section 2 details the data sets and data reduction methods used in this work. In Section 3 the fundamentals of OH airglow emission are examined, and in Section 4 the emission lines used in this work are optimized. In Section 5 the Einstein A coefficients used in this work are listed, and their resultant measured rotational temperatures and populations are detailed. Next, in Section 6 the measured rotational temperatures are compared to SABER VER weighted temperatures, and in

Section 7 the results of this work are compared with previous measurements. Finally, in Section 8, the manuscript concludes with a summary of the results from this analysis.

2. Data

Multiple datasets were used in this analysis. Ground-based observations were acquired from the APOGEE dataset, and night-time space-based observations from SABER, coincident with the ground-based observing site, were also gathered. The observations used in this study span over 2 years, and the complimentary observations allow for a deeper investigation into the effects that the Einstein A coefficients have upon ground-based OH rotational temperature measurements.

2.1. APOGEE

The Sloan Digital Sky Survey (SDSS) APOGEE instrument uses the SDSS dedicated 2.5 m $f/5$ modified Ritchey–Chretien telescope. The SDSS telescope has a 3° diameter field of view with each fiber sub-tending 2 arcseconds in diameter on the sky, and is located at the Apache Point Observatory (APO), Sunspot, New Mexico, USA, latitude 32.78° longitude −105.82°, at an elevation of 2788 m. The APOGEE spectrograph operates from 1.51 to 1.7 µm with a resolution of approximately $r = \lambda/\Delta\lambda \approx 22{,}500$. For more detailed information on the APOGEE spectrograph and its performance, see Wilson et al. [18] or Wilson et al. [19], and for more information on the APOGEE data reduction pipeline, see Nidever et al. [20]. The APOGEE spectrograph is fiber fed by 300 fibers, and typically 35 of the 300 fibers are dedicated to astronomically blank patches of sky which are termed sky fibers. The APOGEE sky spectra are collected for the intended purpose of removing the background atmospheric airglow emission present in astrophysical science spectra during the data reduction process. The APOGEE sky spectra used in this work represent over 4200 observations, totaling nearly 150,000 spectra, taken between June 15, 2011 and June 23, 2013 with each having a 500 second integration time. The APOGEE spectra contain the OH$(4-2)$ and OH$(3-1)$ ro-vibrational transitions from the $\Delta v = -2$ first overtone. In this work we only examined the OH$(4-2)$ transition as it matches the emission sampled by the SABER instrument.

Astronomical spectra are acquired through a range of zenith angles, thus line intensities $I(z)$ are normalized to a zenith observation $I(0)$ using the van Rhijn [21] conversion

$$I(0) = I(z)\sqrt{1 - \left(\frac{R\sin(z)}{R+h}\right)^2}, \tag{1}$$

where h is the height of the emitting layer, assumed to be approximately 87 km, and R is the radius of the Earth. APOGEE spectra are in units of erg/sec/Å/cm^2 which for the further use in intensity calculations were converted to units of Rayleighs per Å. Rayleighs have the dimensions of 10^6 photons/sec/cm^2, and when divided by the corresponding Einstein A coefficient, provide a direct measure of the column density of a species responsible for an emission process at a given wavelength. Rees et al. [22] found that horizontal wind velocities near the mesopause could exceed 100 m/s, and on average were 10 m/s. A single APOGEE spectrum of 500 s integration time would on average sample a volume of air 5 km in length, assuming an average 10 m s^{-1} horizontal wind velocity. The entire field of view of the SDSS telescope is approximately 5 km in diameter at the height of the mesopause, consequently the APOGEE sky spectra in a single observation are effectively sampling overlapping volumes of atmosphere.

2.2. SABER

The Thermosphere Ionosphere Mesosphere Energetics and Dynamics (TIMED) satellite was launched in December of 2001, and has been continuously monitoring the Earth's atmosphere since. The SABER instrument on board the TIMED satellite performs limb scan measurements of the Earth's

atmosphere creating temperature, pressure, density, and VER profiles. In this work SABER data version 1.07 was used, and for a more detailed treatment of the SABER instrument see Russell et al. [23].

SABER measures atmospheric limb emission in 10 broadband radiometer channels ranging from 1.27 to 17 µm, and atmospheric temperature profiles with a 2 km height resolution are derived from 15 µm CO_2 emission measurements. The uncertainties in the SABER CO_2 temperature profiles vary from 1% at 80 km, 2% at 88 km, to over 20% at 110 km, and Garcia-Comas et al. [24] determined that the largest single error in the temperature measurements was due to the uncertainty in the quenching rate of CO_2 by atomic oxygen. Additional information on SABER's kinetic temperature measurements using CO_2 emission can be found in Mertens et al. [25] or Mertens et al. [26].

The SABER channel B measures the OH VER around 1.6 µm which is composed of the $OH(5-3)$ and $OH(4-2)$ ro-vibrational transitions. Noll et al. [3] found an approximately 1 K difference between rotational temperatures measured from the $OH(4-2)$ and $OH(5-3)$ transitions with the $OH(4-2)$ transition being warmer. In the work by Noll et al. [27], they found an effective upper vibrational level $v' = 4.57$ for the SABER channel B, implying that it effectively measured an average VER of the 2 transitions.

All night-time SABER observations that began within a 50 km radius of APO were obtained. The atmospheric profiles from SABER are not measured in a strict vertical sense, but instead ranges nearly 3° in latitude. The largest variations in atmospheric profiles occur in a latitudinal sense, and the SABER measurements used in this work are intended to measure average atmospheric characteristics at a comparable geographic latitude to APO. The SABER observations of APO totaled over 8800 observations from 2001 to 2015. SABER has made approximately 75 observations which occurred during an APOGEE observation, and in these 75 observations there are approximately 2600 spectra.

2.3. Measurement Errors

The APOGEE survey is designed to measure chemical abundances and radial velocities, and unfortunately flux standards are not observed. Consequently, the APOGEE spectra are not flux calibrated in a typical manner. To allow for better sky subtraction, APOGEE corrects for fiber-to-fiber throughput variations which are on the order of 10%. After the throughput variations are corrected, Nidever et al. [20] reports that the flux variations in the OH emission lines are less than 5% over a single observation. Using the histogram of the ratio of two flats taken two years apart, Nidever et al. [20] found the one σ spread of the distribution to be 0.002, which they primarily attribute to photon statistics, showing that the response of the APOGEE instrument is extremely stable over time. After fiber-to-fiber variations are corrected each spectrum is scaled by a wavelength dependent spectral response function to apply an approximate relative flux calibration.

The lack of flux calibration for the APOGEE data would at first appear to be problematic, but this work was focused on measuring OH line temperatures which are more dependent upon relative flux levels of the lines in a single spectrum rather than an absolute flux scale. The measurement of column densities should also not be significantly impacted as it is measured in the rotational temperature calculation process rather than from absolute flux levels.

Fiber-to-fiber variations in a single observation are comprised of instrumental throughput differences, gradients in airglow intensity across the field of view, data reduction errors, and shot noise. In the measurement of the $OH(4-2)$ emission intensity the standard deviation per observation, the standard deviation of all the fibers from a single pointing, was less than 5%. The largest errors in the line measurements in this work are due to errors in the measurement and subtraction of the continuum, and contamination of lines by an adjacent emission line. The standard deviation per observation for all lines considered in this work was less than 1%, and for the measurement of $OH(4-2)$ rotational temperature the standard deviation per observation was at most 3%. The one σ OH flux variations over the entire APOGEE dataset used in this work were approximately 40% which is roughly equivalent in magnitude to the nightly and annual variations in OH emission intensity.

Although the standard deviation of an observation does not give any measure of absolute error, it is a measure of instrumental and data reduction errors. Distributions of the standard deviation per observation for the OH$(4-2)$ intensity is shown in Figure A1 and can be found in Appendix A. The distribution of standard deviation per observation of the OH$(4-2)$ rotational temperatures has also been included for reference in Figure A2. In both Figures A1 and A2, the observation standard deviations have been normalized by their respective observation mean to give the variation in terms of a percentage.

3. OH Emission

Bates and Nicolet [28] found that the OH molecule is primarily created by the ozone hydration reaction

$$\mathrm{H} + \mathrm{O_3} \rightarrow \mathrm{OH}(\mathrm{v} \leq 9) + \mathrm{O_2} \tag{2}$$

which occurs around an altitude of 87 km, near the mesopause, in a narrow layer of approximately 10 km in height. Charters et al. [29], Llewellyn et al. [30], and Ohoyama et al. [31] found that the reaction in Equation (2) produces OH molecules in the 9^{th}, 8^{th}, and 7^{th} vibrational states. Vibrational relaxation of the OH molecule are due to radiative transitions and collisional relaxation.

Each vibrational level of the OH molecule is accompanied by a range of rotational states. Radiative vibrational relaxations are typically accompanied by a change in rotational angular momentum termed ro-vibrational transitions. The selection rules for the rotational transitions are $\Delta j = 0, \pm 1$, giving rise to Q, P, and R branches. The R branch transitions correspond to $\Delta j = -1$ with $\Delta j = j'' - j'$, where j'' is the final rotational state and j' is the initial. The Q branch transitions correspond to $\Delta j = 0$, and the P branch transitions correspond to $\Delta j = +1$. Figure 1 is the median APOGEE OH$(4-2)$ spectrum with emission lines from the P branch labeled.

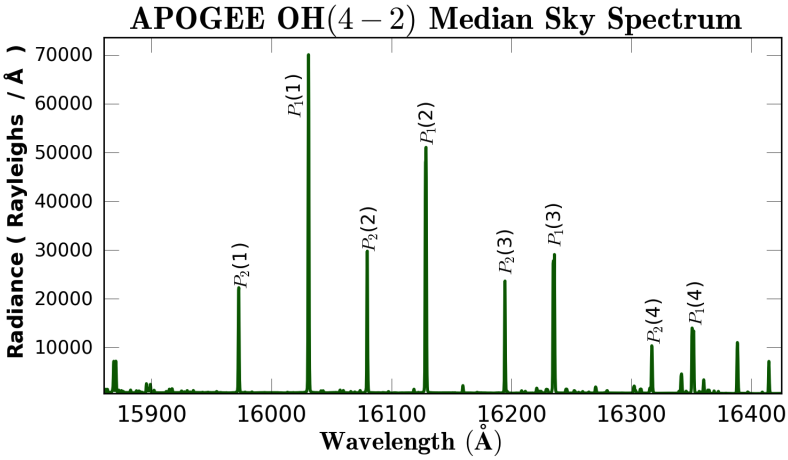

Figure 1. Median APOGEE sky spectrum of the OH$(4-2)$ transition with electronic sub-states and quantum numbers N' labeled for each emission line.

OH emission in the optical and infrared is from the ground electronic state, and is composed of two sub-states. This multiplet structure, referred to as spin-splitting, is an effect that occurs due to the interaction between the electron spin vector and the projection of the orbital angular momentum vector along the internuclear axis. The P_1 transitions correspond to the electronic sub-state F_1, which have a total of $3/2$ electron spin and orbital angular momentum projected onto the internuclear axis. Whereas the P_2 transitions correspond to the electronic sub-state F_2, which have a projected total angular momentum of $1/2$. The ground electronic state of the OH molecule is inverted as the energy levels of the F_1 states are lower than the energy levels of the F_2 states, and the emission lines of the P_1 transitions are brighter than the emission lines of the P_2 transitions. Although some OH molecules do

make transitions from the F_1 to the F_2 state, and vice versa, these transitions are rare and too faint to be observed in the APOGEE spectra.

The value in parenthesis in Figure 1 is the rotational quantum number of the upper state. A common notation used in molecular spectroscopy uses N', where $N' = 1$ represents the lowest final total angular momentum state for the branch. In the case for $P_1(N' = 1)$ the total final angular momentum is $j'' = 2.5$, and for $P_2(N' = 1)$ the total final angular momentum is $j'' = 1.5$.

The coupling of rotational motion further splits the F_1 and F_2 sub-states. Λ doubling splits each energy level into e and f components. The APOGEE spectra are of sufficient resolution to begin resolving some of the Λ doublets with a resolution element having a width of 0.6 Å at 1.5 µm. Osterbrock et al. [32], in their line atlas, only list Λ doublets with spacings greater than 0.2 Å, and Rousselot et al. [33], in their line atlas, use a 1 Å threshold. Due to the rotational coupling nature of the Λ doublets, the spacing of the doublets increases with increasing angular momentum. In Figure 1 the $P_1(3)$ and $P_1(4)$ emission lines both have resolved Λ doublets each with a spacing in excess of 1 Å.

OH Rotational Temperature

For an OH vibrational level in thermal equilibrium with the surrounding atmosphere, the populations of the lower rotational states are well described by an isothermal Boltzmann distribution

$$N_{v'j'} = N_0 g_i \left(2j' + 1\right) \exp\left(\frac{-hcF(j')}{kT}\right), \tag{3}$$

where N_0 is the population of the lowest rotational state of the vibrational level v', $g_i = 2$ is the electronic degeneracy, the $2 \cdot j' + 1$ term represents the degeneracy of the rotational states, k is the Boltzmann constant, $F(j')$ is the rotational term value of the upper state in units of cm^{-1}, and T is the rotational temperature in Kelvins. The column density of the OH$(v'j')$ state is given by

$$N_{v'j'} = \frac{I^{v'j'}_{v''j''}}{A^{v'j'}_{v''j''}}, \tag{4}$$

where $I^{v'j'}_{v''j''}$ is the measured intensity of the OH transition in Rayleighs, $A^{v'j'}_{v''j''}$ is the Einstein A coefficient for the particular transition in units of s^{-1}, (v', j') is the initial vibrational and rotational state, and (v'', j'') is the final state. Rotational temperatures are determined by measuring the slope of a linear fit to $\ln\left(\frac{I^{v'j'}_{v''j''}}{2(2j'+1)A^{v'j'}_{v''j''}}\right)$ versus $F(j')$ as similarly performed by Cosby and Slanger [2] and Noll et al. [3]. The population of the lowest rotational level, N_0, is derived from the intercept of the rotational fit, and to accomplish this the energy of the $P_1(1)$ emission line is shifted to zero energy. Lastly, the other emission lines are shifted by the same amount.

4. Emission Line Selection

The measurement of the line intensity was performed by integrating the area under the line after the continuum was estimated and subtracted. Emission lines that are blended with another emission line or absorption feature, or which originate from rotational levels whose populations are not in LTE, may skew an OH rotational temperature measurement. To determine the effect emission line selection had upon OH rotational temperature measurements, an analysis was undertaken. For a given combination of emission lines the mean APOGEE OH$(4-2)$ rotational temperature and column density was measured. In Table 1, the eleven combinations of emission lines along with their resultant mean rotational temperature and column density are listed.

The night sky atlas by Rousselot et al. [33] reveals that the $P_2(4)$ emission line is blended with an emission line from the R branch of the OH$(5-3)$ transition, and Table 1 shows that this line

significantly increased the mean rotational temperature, and for these reasons this line was rejected from further temperature calculations. In Table 1, it can be seen that all lines for which $N' \geq 3$ in both the P_1 and P_2 branches, effectively increased measured rotational temperatures. To minimize systematic errors in rotational temperature measurements only the $N' \leq 2$ emission lines of the P_1 and P_2 branches were used.

Table 1. Table of mean APOGEE OH$(4-2)$ rotational temperatures and column densities as a function of emission line selection. The Einstein A coefficients of Mies were used for all calculations. The top row of the table lists the emission lines considered with the last two columns representing the resultant measured mean temperature and column density. Emission lines marked with an 'X' were used in that combination.

$P_1(1)$	$P_1(2)$	$P_1(3)$	$P_1(4)$	$P_2(1)$	$P_2(2)$	$P_2(3)$	$P_2(4)$	Temp (K)	N_0 (10^6 molecules/cm^2)
X	X			X	X			195.0	1775.0
X	X	X		X	X			197.7	1767.6
X	X			X	X	X		199.1	1757.4
X	X		X	X	X			201.1	1742.0
X	X			X	X		X	206.1	1720.4
X	X	X		X	X	X		199.8	1759.7
X	X	X	X	X	X	X		201.9	1745.8
X	X	X		X	X	X	X	205.3	1722.7
X	X	X	X	X	X	X	X	205.2	1722.9
X	X		X	X	X	X	X	205.2	1722.7
X	X	X	X	X	X		X	205.8	1722.7

5. Einstein A Coefficients

Using the selected lines from Section 4, the OH$(4-2)$ rotational temperatures were measured for the entire APOGEE dataset using five sets of Einstein A coefficients. The Einstein A coefficients tested were from Mies [6], Turnbull and Lowe [8], Rothman et al. [17], van der Loo and Groenenboom [16], and Langhoff [7]. These Einstein A coefficients will hereafter be referred to as Mies, TL, HITRAN, Loo, and LWR, respectively, and are listed in Table 2. The distributions of measured OH$(4-2)$ rotational temperatures versus Einstein A coefficient are shown in Figure 2, and four of the five sets of Einstein A coefficients measured a mean OH$(4-2)$ rotational temperature of approximately 195 K with only the LWR coefficients deviating significantly. The Einstein A coefficients had a minimal impact upon the shape of the temperature distributions, but instead shifted the centers of the distributions. The distributions of APOGEE OH$(4-2)$ rotational temperatures also appear to be bimodal.

Table 2. Table of Einstein A coefficients for the P branch of OH$(4-2)$. The Einstein A coefficients have units of s^{-1} and are from Mies [6], Turnbull and Lowe [8], Rothman et al. [17], van der Loo and Groenenboom [16], and Langhoff [7] with these coefficients being labeled Mies, TL, HITRAN, Loo, and LWR respectively.

Δv	Transition	j″	Mies	TL	HITRAN	Loo	LWR
4-2	$P_1(1)$	2.5	30.419	29.654	20.89	18.817	18.287
	$P_1(2)$	3.5	37.037	35.961	25.60	23.114	22.553
	$P_1(3)$	4.5	39.717	38.410	27.59	24.996	24.464
	$P_1(4)$	5.5	41.236	39.704	28.77	26.158	25.661
	$P_2(1)$	1.5	48.139	47.248	32.91	29.558	29.767
	$P_2(2)$	2.5	44.658	43.716	30.75	27.719	27.289
	$P_2(3)$	3.5	43.757	42.667	30.32	27.430	27.404
	$P_2(4)$	4.5	43.636	42.369	30.41	27.614	27.519

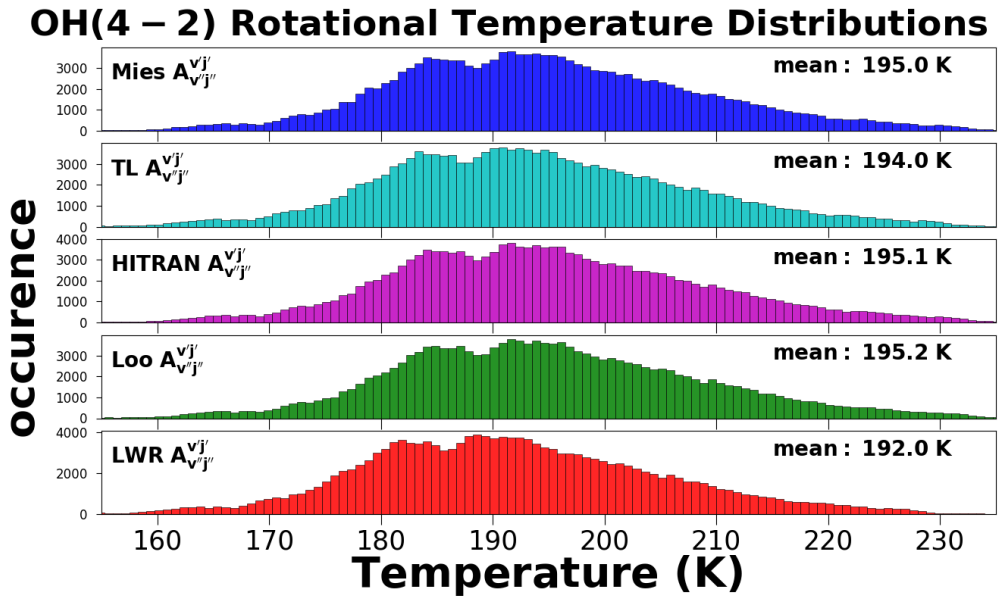

Figure 2. APOGEE OH$(4-2)$ rotational temperature distributions versus Einstein A coefficients.

Figure 3 shows the distributions of the measured N_0 populations for each of the Einstein A coefficients in consideration. The N_0 populations were derived from the intercept of the rotational temperature fit. The five sets of Einstein A coefficients tested here yielded mean column densities which ranged from $1.7 \cdot 10^9$ to $3 \cdot 10^9$ molecules/cm^2.

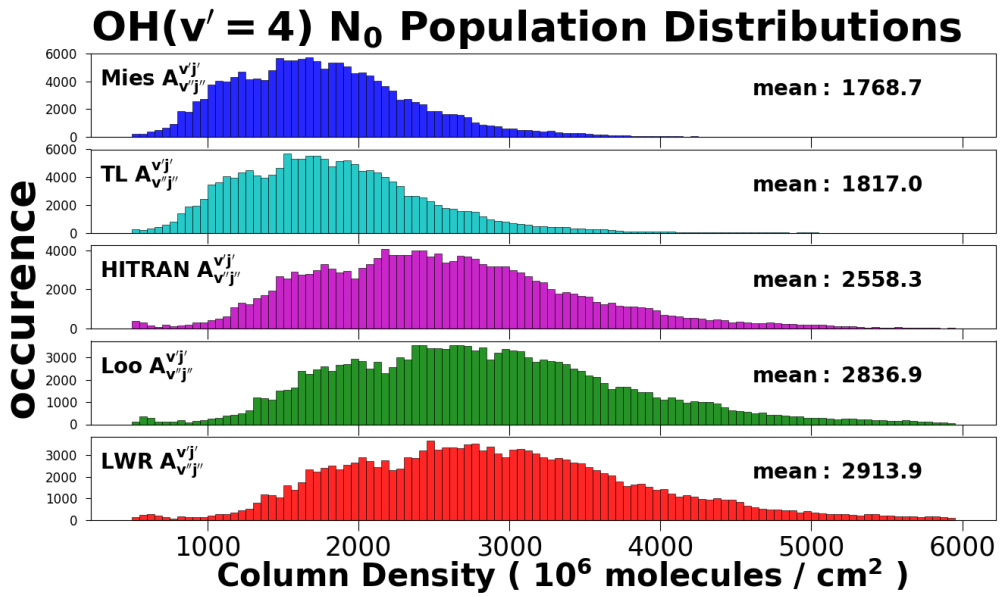

Figure 3. The distributions of N_0 population versus Einstein A coefficients for the APOGEE data set.

The median APOGEE OH$(4-2)$ spectrum in Figure 1 is a robust measure of the OH$(4-2)$ emission above APO. The rotational temperature of the median OH$(4-2)$ spectrum was calculated using the 5 sets of Einstein A coefficients in Figure 4. Four of the five sets of Einstein A coefficients did not significantly impact the temperature measurement as they found a mean temperature of approximately 195 K with only the coefficients of LWR significantly deviating. It can also be seen in Figure 4 that the $N' \geq 3$ lines all show signs of enhancement due to non-LTE effects.

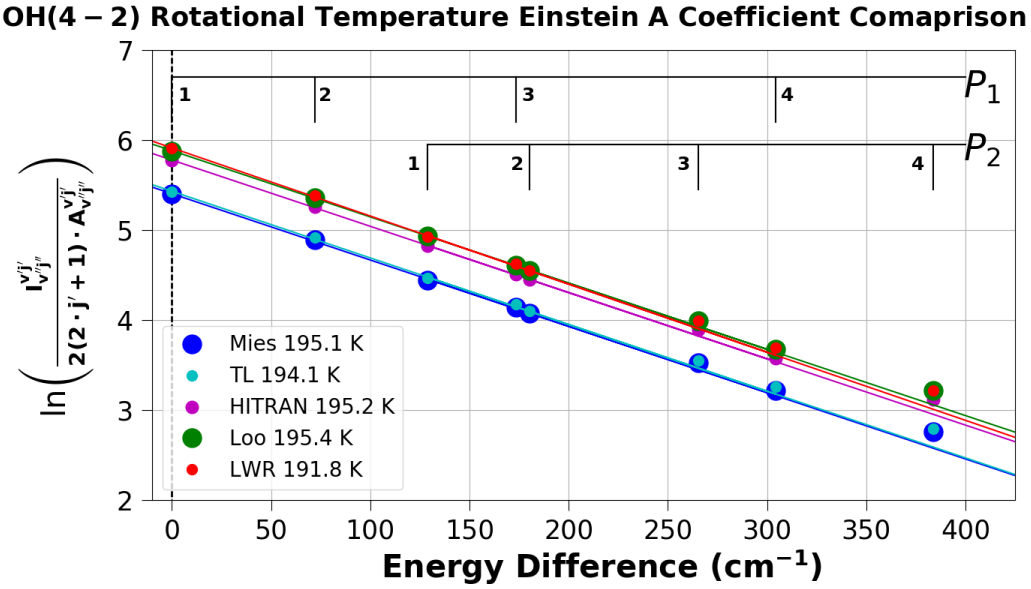

Figure 4. The rotational temperature measurements of the median OH$(4-2)$ spectrum in Figure 1 calculated using the Einstein A coefficients from Mies, TL, HITRAN, Loo, and LWR. The rotational temperatures were calculated using the $N' \leq 2$ emission lines of the P_1 and P_2 branches.

The Einstein A coefficients had a significant impact upon the value of the intercept which represents the population of N_0. Table 3 lists the populations calculated from the median APOGEE OH$(4-2)$ spectrum in Figure 1 using the Einstein A coefficients from Mies, TL, HITRAN, Loo, and LWR. Line 1 of Table 3 is the log of the population of N_0, and line 2 is the column density in units of 10^6 molecules/cm^2. Line 3 is the ratios of the N_0 populations normalized by $N_{0,Mies}$. The calculated populations of the Mies and TL coefficients differ by approximately 3%. Although the LWR and Loo populations differ by less than 10%, they are both approximately 60% greater than the populations calculated using the Mies coefficients. In Table 1, it can be seen that the line selection did not have a significant effect upon the measured population of N_0.

Table 3. The N_0 populations of the median OH$(4-2)$ spectrum in Figure 1 calculated using the Einstein A coefficients of Mies, TL, HITRAN, Loo, and LWR. Line 1 of the table is log of the population of N_0, and line 2 is the column density in units of 10^6 molecules/cm^2. Line 3 is the ratios of the N_0 populations normalized by $N_{0,Mies}$.

	Mies	TL	HITRAN	Loo	LWR
$ln\left(\frac{N_0}{2\cdot(2\cdot j'+1)}\right)$	5.40	5.43	5.77	5.87	5.90
N_0	1771	1825	2564	2833	2920
N_0 / $N_{0,Mies}$	1	1.030	1.462	1.616	1.665

The columns of Einstein A coefficients of Mies, TL, HITRAN, Loo, and LWR, in Table 2, have been ordered from the largest numerically to the smallest. The Mies coefficients are the largest of the Einstein A coefficients considered in this work, and the coefficients of LWR are the smallest. The distributions in Figures 2 and 3 are also ordered from the largest set of coefficients to the smallest, and clear trends in the rotational temperatures and N_0 populations are evident. The coefficients of Mies, TL, HITRAN, and Loo show little difference in mean rotational temperature while the coefficients of LWR measured lower rotational temperatures. The Mies coefficients being the largest numerically measure the lowest mean N_0 population; in contrast, the LWR coefficients measure the largest mean N_0 population.

Equation (4) shows that the column density of a rotational state is inversely proportional to the Einstein A coefficient with the larger coefficients yielding smaller column densities. The linear fit of

log population to rotational energy used in rotational temperature measurements is sensitive to the ratio of the column densities and not sensitive to constant offsets. The natural log of the density is a slowly varying function which helps to minimize the differences between the sets of the Einstein A coefficients. A change in the ratios of the coefficients translates into deviations of the slope, and the rotational temperature is inversely proportional to the slope of the linear fit.

In an attempt to gain a better understanding of the differences between the sets of Einstein A coefficients, the coefficients were normalized by their respective $P_1(1)$ coefficient and plotted versus their corresponding rotational energy in Figure 5. The ratios of the P_1 coefficients of TL are always the smallest, and the ratios of LWR coefficients are the greatest. All of the P_1 coefficient ratios increase in a way such that they do not cross the ratio of another set of coefficients. Contrastingly, the ratios of the P_2 coefficients do cross. Ignoring the P_2 coefficient ratios of LWR, the P_2 coefficient ratios of Loo are the smallest at lower rotational energies and the largest at higher rotational energies. In Figure 5, the coefficient ratios of Mies and TL are similar, as are the coefficient ratios of Loo and HITRAN. The ratio of the LWR coefficients are consistently greater than the other four coefficients in consideration, and the greater coefficient ratio translates into a lower measured rotational temperature and a larger calculated N_0 population.

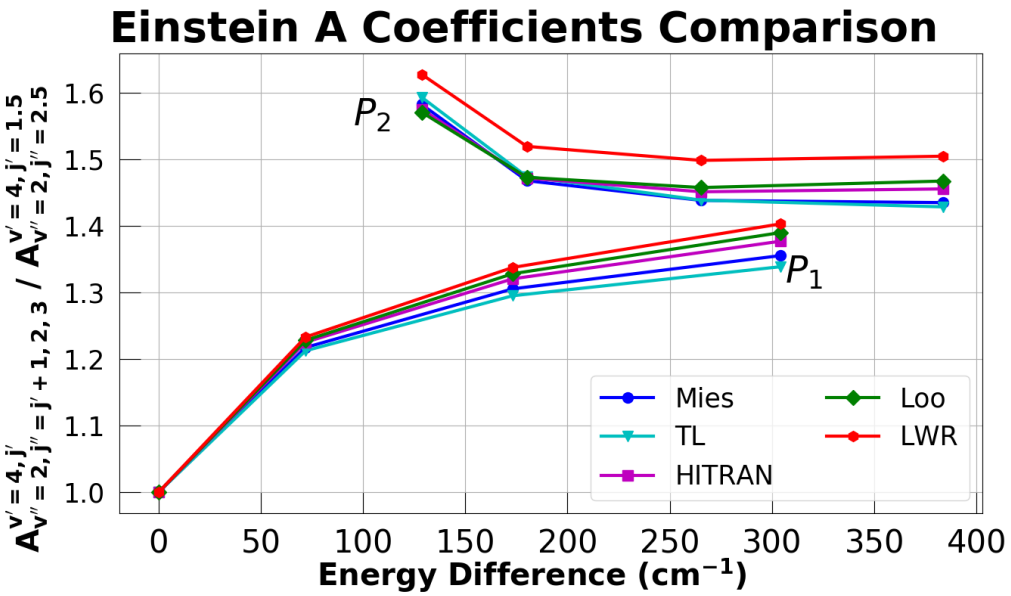

Figure 5. The five sets of Einstein A coefficients compared. Each set of Einstein A coefficients have been normalized by their $P_1(1)$ coefficient to allow for a comparison.

6. SABER Comparison

Ground-based OH rotational temperature measurements are sampling a column of atmosphere, and in effect measure a vertical VER profile weighted average temperature. While SABER on the other hand measures a temperature profile. To allow for a proper comparison, Liu et al. [10] weighted the SABER temperature profiles using the corresponding SABER OH 1.6 μm VER profiles as in Equation (5).

$$T_{SABER} = \frac{\sum_z T(z) \cdot VER_{1.6\mu m}(z)}{\sum_z VER_{1.6\mu m}(z)} \quad (K) \tag{5}$$

The altitude at which the OH emission peaks varies with vibrational level, and as both SABER and APOGEE sample emission from the OH$(4-2)$ transition the VER weighted temperatures should not be significantly biased due to differences in the altitude of emission. Small-scale spatial variations are probably still a significant source of error in comparing the two measurements as APOGEE measures a

vertical column and SABER measures a vertical profile in a sweeping motion which ranges nearly 3° in latitude.

To test the accuracy of the ground-based OH$(4-2)$ rotational temperature measurements, the difference between the SABER VER weighted temperatures and OH rotational temperatures were calculated, and Figure 6 shows the distribution of these temperature differences versus Einstein A coefficient. The average temperature difference between APOGEE and SABER is approximately 1 K, and is the smallest for the Einstein A coefficients by LWR. The APOGEE OH$(4-2)$ rotational temperatures are on average higher than the SABER temperatures.

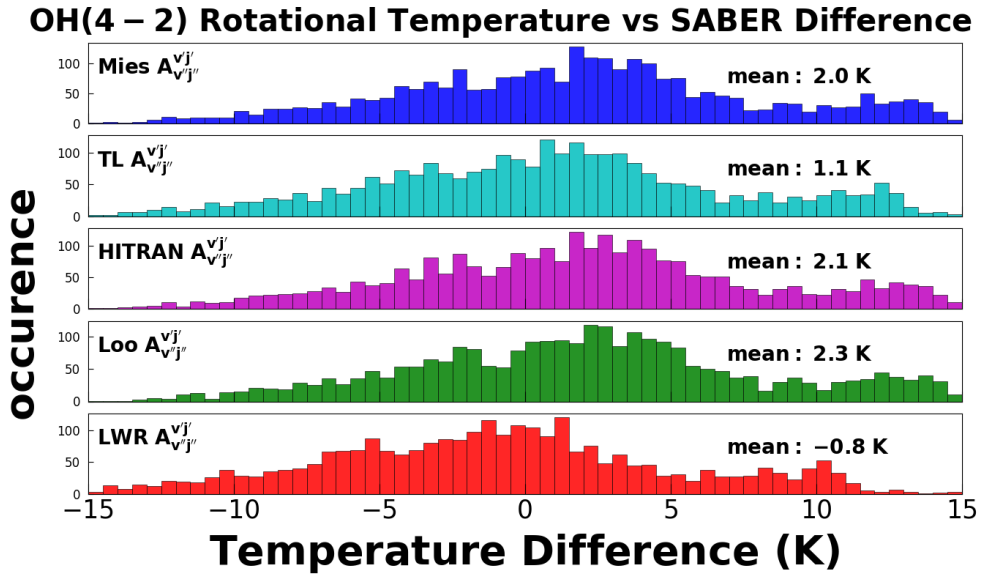

Figure 6. The distribution of the temperature differences between the APOGEE OH$(4-2)$ rotational temperatures and the SABER VER weighted temperatures.

7. Discussion

Using optical SDSS spectra, Hart [4] measured a median OH$(4-0)$ rotational temperature at APO of approximately 195 K using the coefficients of van der Loo and Groenenboom [16]. In this work, the mean APO OH$(4-2)$ rotational temperature was approximately 195 K using the same coefficients. For the rotational temperature measurements the coefficients of Mies, TL, HITRAN, and Loo yielded nearly identical OH$(4-2)$ rotational temperatures, and the coefficients of LWR yielded consistently lower rotational temperatures.

French et al. [34] tested the coefficients of Mies, TL, and LWR. They determined that the coefficients of LWR best matched experimentally measured temperatures. However, French et al. [34] used the ratio of emission lines to measure rotational temperatures, and they did not use any ratios containing an emission line from the P_2 branch where the LWR coefficients are significantly different from the other sets of coefficients as evidenced by Figure 5.

Measuring the rotational temperature of multiple transitions from the same upper vibrational level Noll et al. [3] analyzed the coefficients of Goldman et al. [9] and van der Loo and Groenenboom [16]. They found the coefficients of Goldman et al. [9] resulted in less scatter between the rotational temperatures derived from multiple overtones originating from the same upper vibrational level.

In this work, the average temperature difference between APOGEE and SABER was observed to be slightly greater than 1 K, with the APOGEE OH$(4-2)$ rotational temperatures being predominately higher than the SABER VER weighted temperatures. Liu et al. [10] examined the same coefficients as this work, and found the LWR coefficients most closely matched the SABER data. Using the LWR coefficients Liu et al. [10] measured the OH$(6-2)$, OH$(5-1)$, and OH$(3-0)$ rotational temperatures using the N$'$ = 1, 2, and 3 rotational levels of the P_1 branch, and found a positive 2.7 K, 1.4 K, and

2.1 K bias, respectively, and a positive 9.6 K bias for the $OH(8-3)$ rotational temperature using the N′ = 1, 2, and 4 rotational levels of the P_1 branch. The results of Liu et al. [10] showed a more significant differences in the calculated rotational temperatures between the Einstein A coefficients in comparison to this work. Liu et al. [10] found that the LWR coefficients had the smallest bias in comparison to SABER VER weighted temperatures, and an examination of Figure 5 shows that the LWR coefficients differ significantly from the other coefficients tested in the P_2 branch. Also all of the transitions Liu et al. [10] compared to SABER data are from higher overtones.

French and Mulligan [35] compared SABER temperatures to $OH(6-2)$ rotational temperatures in Davis Antarctica. They found less than 2 K difference from SABER temperatures using the coefficients of LWR utilizing the same method of OH rotational temperature measurement as employed in French et al. [34]. French and Mulligan [35] initially considered all SABER observations in which the tangent point was within 500 km of Davis, and later switched to a more restrictive 100 km and found little change in the SABER versus ground-based OH rotational temperature biases. They concluded that the OH layer was largely uniform over these length scales.

The five sets of Einstein A coefficients tested in this work yielded mean N_0 column densities which ranged from $1.7 \cdot 10^9$ to $3 \cdot 10^9$ molecules/cm^2 for the $v' = 4$ vibrational level of the OH molecule. Dodd et al. [36] found the $v' = 4$ column densities to be approximately $2 \cdot 10^9$ molecules/cm^2 using the coefficients of Nelson et al. [12], which are comparable to the HITRAN coefficients. Cosby and Slanger [2] measured the $v' = 4$ column densities to be approximately $3.5 \cdot 10^9$ molecules/cm^2 using the coefficients of Goldman et al. [9]. The coefficients of Goldman et al. [9] with minor modifications are the HITRAN coefficients of Rothman et al. [17].

8. Conclusions

Using the APOGEE $OH(4-2)$ ro-vibrational emission spectra, an analysis was performed to determine the effect that the Einstein A coefficients have upon ground-based rotational temperature measurements. Four of the five sets of Einstein A coefficients tested yielded statistically identical mean rotational temperatures of approximately 195 K for the $OH(4-2)$ transition. Using the coefficients of Loo, the average $OH(4-2)$ rotational temperature over the period of June 2011 to June 2013 at APO was found to be 195 K. The Einstein A coefficients had a significant impact upon the measured $OH(v' = 4)$ vibrational populations. The coefficients of HITRAN, Loo, and LWR yielded $OH(v' = 4)$ populations over 50% greater than the coefficients of Mies and TL.

The Einstein A coefficients of LWR consistently measure lower OH rotational temperatures. As the ground-based rotational temperatures are typically higher than space-based measurements, due to non-LTE effects, the LWR coefficients are consequently the best match to the SABER VER weighted temperatures. In this work, the difference between SABER temperatures and OH rotational temperatures was on average 1 K. The non-LTE effects were a larger source of error for OH rotational temperature measurements than the Einstein A coefficients. In contrast the Einstein A coefficients were found to have a larger effect upon column density measurements than non-LTE effects.

Funding: This research received no external funding.

Acknowledgments: The author must first acknowledge the reviewers for their patience and enormous amount of assistance. Without their gracious help, this manuscript would not have been possible. We would also like to thank the TIMED/SABER science teams for providing the atmospheric profile data used in this study. All data analysis performed for this work was done in python using Enthought Python Distribution's (EPD) CanoPy V1.6.1. The primary packages used in conjunction with CanoPy were NumPy 1.11.3, PyFITS 3.3, SciPY 1.0.0, MatPlotLib 2.0.0, AstroPY 2.0.12, and SciKit-Learn 0.19.1. TeXstudio 2.11.0 was used to type set this manuscript. Funding for SDSS-III has been provided by the Alfred P. Sloan Foundation, the Participating Institutions, the National Science Foundation, and the U.S. Department of Energy Office of Science. The SDSS-III web site is http://www.sdss3.org/. SDSS-III is managed by the Astrophysical Research Consortium for the Participating Institutions of the SDSS-III Collaboration including the University of Arizona, the Brazilian Participation Group, Brookhaven National Laboratory, Carnegie Mellon University, University of Florida, the French Participation Group, the German Participation Group, Harvard University, the Instituto de Astrofisica de Canarias, the Michigan State/Notre Dame/JINA Participation Group, Johns Hopkins University, Lawrence Berkeley National Laboratory,

Max Planck Institute for Astrophysics, Max Planck Institute for Extraterrestrial Physics, New Mexico State University, New York University, Ohio State University, Pennsylvania State University, University of Portsmouth, Princeton University, the Spanish Participation Group, University of Tokyo, University of Utah, Vanderbilt University, University of Virginia, University of Washington, and Yale University.

Conflicts of Interest: The author declares no conflicts of interest.

Appendix A. Supplemental Plots

The distribution of the standard deviation per observation for the emission intensity is shown in Figure A1, and the distribution of standard deviation per observation of rotational temperatures has also been included for reference in Figure A2. In Figures A1 and A2, the observation standard deviations have been normalized by their respective observation mean to give the variation in terms of a percentage.

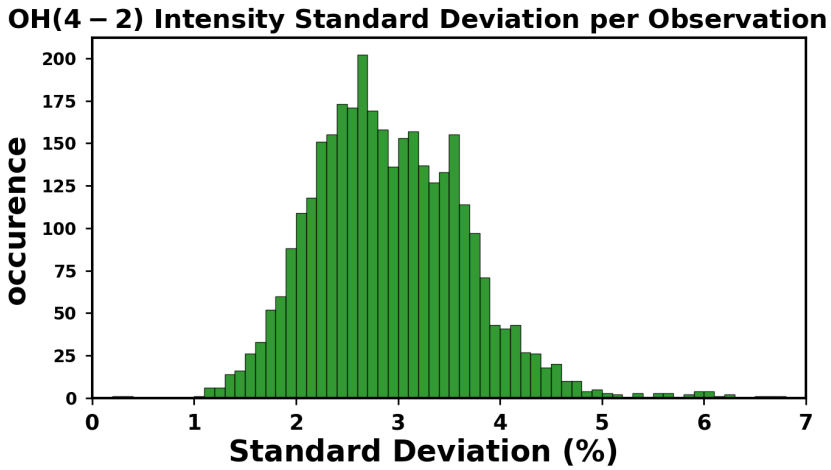

Figure A1. Standard deviation per observation of the OH$(4-2)$ emission intensity for the APOGEE data set.

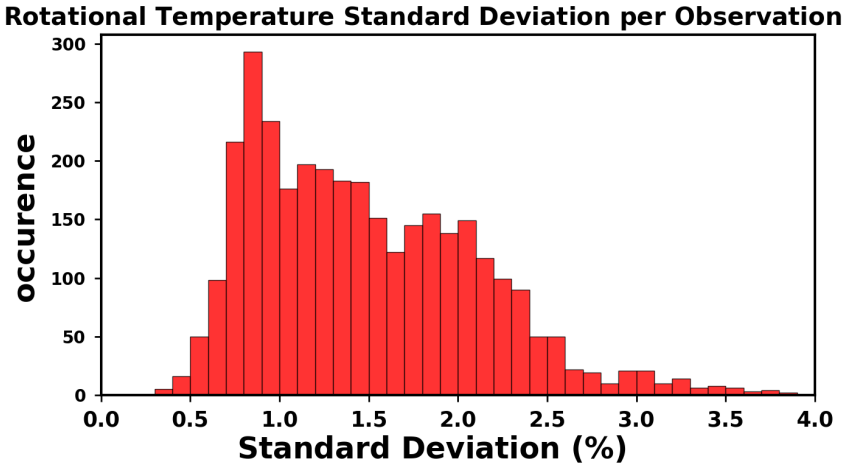

Figure A2. Standard deviation per observation of the OH$(4-2)$ rotational temperature for the APOGEE data set.

References

1. Von Savigny, C.; McDade, I.C.; Eichmann, K.U.; Burrows, J.P. On the dependence of the OH* Meinel emission altitude on vibrational level: SCIAMACHY observations and model simulations. *Atmos. Chem. Phys.* **2012**, *12*, 8813–8828. [CrossRef]
2. Cosby, P.C.; Slanger, T.G. OH spectroscopy and chemistry investigated with astronomical sky spectra. *Can. J. Phys.* **2007**, *85*, 77–99. [CrossRef]
3. Noll, S.; Kausch, W.; Kimeswenger, S.; Unterguggenberger, S.; Jones, A.M. OH populations and temperatures from simultaneous spectroscopic observations of 25 bands. *Atmos. Chem. Phys.* **2015**, *15*, 3647–3669. [CrossRef]
4. Hart, M. Long-term Spectroscopic Observations of the Atmospheric Airglow by the Sloan Digital Sky Survey. *Publ. Astron. Soc. Pac.* **2018**, *131*, 1–25. [CrossRef]
5. Pendleton, W.R.; Espy, P.J.; Hammon, M.R. Evidencefor Non-Local-Thermodynamic-Equilibrium Rotation in the OH Nightglow. *J. Geophys. Res.* **1993**, *98*, 11567–11579. [CrossRef]
6. Mies, F.H. Calculated Vibrational Transition Probabilities of OH ($X^2\Pi$). *J. Mol. Spectrosc.* **1974**, *53*, 150–188. [CrossRef]
7. Langhoff, S. Theoretical Transition Probabilities for the OH Meinel System. *J. Mol. Spectrosc.* **1986**, *118*, 507–529. [CrossRef]
8. Turnbull, D.N.; Lowe, R.P. New Hydroxyl Transition Probabilities and Their Importance in Airglow Studies. *Planet. Space Sci.* **1988**, *37*, 723–738. [CrossRef]
9. Goldman, A.; Schoenfeld, W.G.; Goorvitch, D.; Chackerian, C.; Dothe, H.; Melen, M.; Abrams, M.C.; Selby, J.E.A. Updated Line Parameters for OH X^2II-X^2II(v",v') Transitions. *J. Quant. Spectrosc. Radiat. Transf.* **1998**, *59*, 453–469. [CrossRef]
10. Liu, W.; Xu, J.; Smith, A.K.; Yuan, W. Comparison of rotational temperature derived from ground-based OH airglow observations with TIMED/SABER to evaluate the Einstein coefficients. *J. Geophys. Res. Space Phys.* **2015**, *10*, 1–14. [CrossRef]
11. Stevens, W.J.; Das, G.; Wahl, A.C.; Krauss, M.; Neumann, D. Study of the ground state potential curve and dipole moment of OH by the method of optimized valence configurations. *J. Chem. Phys.* **1974**, *61*, 3686–3699. [CrossRef]
12. Nelson, D.D., Jr.; Schiffman, A.; Nesbitt, D.J.; Orlando, J.J.; Burkholder, J.B. H+O_3 Fourier transform infrared emission and laser absorption studies of OH ($X^2\Pi$) radical: An experimental dipole moment function and state to state Einstein *A* coefficients. *J. Chem. Phys.* **1990**, *93*, 7003–7019. [CrossRef]
13. Abrams, M.C.; Davis, S.P.; Rao, M.L.; Engelman, R.; Brault, J. High-Resolution Fourier Transform Spectroscopy of the Meinel System of OH. *Astrophys. J. Suppl. Ser.* **1994**, *93*, 351–395. [CrossRef]
14. Melen, F.; Sauval, A.J.; Grevesse, N.; Farmer, C.B.; Servais, C.; Delbouille, L.; Roland, G. A New Analysis of the OH Radical Spectrum from Solar Infrared Observations. *J. Mol. Spectrosc.* **1995**, *174*, 490–509. [CrossRef]
15. Chackerian, C.; Goorvitch, D.; Benidar, A.; Farreno, R.; Guelachvili, G.; Martin, P.M.; Abrams, M.C.; Davis, S.P. Rovibrational Intensities and Electric Dipole Moment Functions of the $X^2\Pi$ Hydroxyl Radical. *J. Quant. Spectrosc. Radiat. Transf.* **1992**, *48*, 667–673. [CrossRef]
16. Van der Loo, M.P.J.; Groenenboom, G.C. Theoretical transition probabilities for the OH Meinel system. *J. Chem. Phys.* **2007**, *126*, 1–7. [CrossRef] [PubMed]
17. Rothman, L.S.; Gordon, I.E.; Barbe, A.; Benner, D.C.; Bernath, P.F.; Birk, M.; Boudon, V.; Brown, L.R.; Campargue, A.; Champion, J.P.; et al. The HITRAN 2008 molecular spectroscopic database. *J. Quant. Spectrosc. Radiat. Transf.* **2009**, *110*, 533–572. [CrossRef]
18. Wilson, J.C.; Hearty, F.; Skrutskie, M.F.; Majewski, S.; Schiavon, R.; Eisenstein, D.; Gunn, J.; Blank, B.; Henderson, C.; Smee, S.; et al. The Apache Point Observatory Galactic Evolution Experiment (APOGEE) high-resolution near-infrared multi-object fiber spectrograph. *Proc. SPIE* **2010**, *77351*, 77351C.
19. Wilson, J.C.; Hearty, F.R.; Skrutskie, M.F.; Majewski, S.R.; Holtzman, J.A.; Eisenstein, D.; Gunn, J.; Blank, B.; Henderson, C.; Smee, S.; et al. The Apache Point Observatory Galactic Evolution Experiment. *Publ. Astron. Soc. Pac.* **2019**, *131*, 1–76. [CrossRef]
20. Nidever, D.L.; Holtzman, J.A.; Prieto, C.A.; Beland, S.; Bender, C.; Bizyaev, D.; Burton, A.; Desphande, R.; Fleming, S.W.; Pérez, A.E.G.; et al. The Data Reduction Pipeline for the Apache Point Observatory Galactic Evolution Experiment. *Astron. J.* **2015**, *150*, 1–23. [CrossRef]

21. Van Rhijn, P.J. On the Brightness of the Sky at Night and the Total Amount of Starlight. *Publ. Astron. Lab. Gron.* **1921**, *31*, 1–87. [CrossRef]
22. Rees, D.; Aruliah, A.; Fuller-Rowell, T.J.; Wickwar, V.B.; Sica, R.J. Winds in the upper mesosphere at mid-latitude: First results using an imaging Fabry-Perot Interferometer. *Geophys. Res. Lett.* **1990**, *17*, 1259–1262. [CrossRef]
23. Russell, J.M., III; Mlynczak, M.G.; Gordley, L.L.; Tansock, J.J., Jr.; Esplin, R.W. Overview of the SABER experiment and preliminary calibration results. *Proc. SPIE* **1999**, *3756*. [CrossRef]
24. Garcia-Comas, M.; Lopez-Puertas, M.; Marshall, B.T.; Wintersteiner, P.P.; Funke, B.; Bermejo-Pantaleón, D.; Mertens, C.J.; Remsberg, E.E.; Gordley, L.L.; Mlynczak, M.G.; et al. Errors in Sounding of the Atmosphere using Broadband Emission Radiometry (SABER) kinetic temperature caused by non-local-thermodynamic-equilibrium model parameters. *J. Geophys. Res.* **2008**, *113*, 1–16. [CrossRef]
25. Mertens, C.J.; Mlynczak, M.G.; Lopez-Puertas, M.; Wintersteiner, P.P.; Picard, R.H.; Winick, J.R.; Gordley, L.L.; Russell, J.M., III. Retrieval of mesospheric and lower thermospheric kinetic temperature from measurements of CO_2 15 μm Earth limb emission under non-LTE conditions. *Geophys. Res. Lett.* **2001**, *28*, 1391–1394. [CrossRef]
26. Mertens, C.J.; Russell, J.M., III; Mlynczak, M.G.; She, C.Y.; Schmidlin, F.J.; Goldberg, R.A.; López-Puertas, M.; Wintersteiner, P.P.; Picard, R.H.; Winick, J.R.; et al. Kinetic temperature and carbon dioxide from broadband infrared limb emission measurements taken from the TIMED/SABERinstrument. *Adv. Space Res.* **2009**, *43*, 15–27.
27. Noll, S.; Kausch, W.; Kimeswenger, S.; Unterguggenberger, S.; Jones, A.M. Comparison of VLT/X-shooter OH and O_2 rotational temperatures with consideration of TIMED/SABER emission and temperature profiles. *Atmos. Chem. Phys.* **2016**, *16*, 5021–5042. [CrossRef]
28. Bates, D.R.; Nicolet, M. The Photochemsitry of Atmospheric Water Vapor. *J. Geophys. Res.* **1950**, *55*, 301–326. [CrossRef]
29. Charters, P.E.; Macdonald, R.G.; Polanyi, J.C. Formation of Vibrationally Excited OH by the Reaction H + 0_3. *J. Opt.* **1971**, *10*, 1747–1754.
30. Llewellyn, E.J.; Long, B.H.; Solheim, B.H. The Quenching of OH^* in the Atmosphere. *Planet Space Sci.* **1978**, *26*, 525–531. [CrossRef]
31. Ohoyama, H.; Kasai, T.; Yoshimura, H.; Kimura, H.; Kuwata, K. Inital Distribution of Vibration of the OH Radicals Produced in the $H+O_3$->$OH(X^2\Pi)+O_2$ Reaction. Chemiluminescence by a Crossed Beam Technique. *Chem. Phys. Lett.* **1985**, *118*, 263–266. [CrossRef]
32. Osterbrock, D.; Fullbright, J.; Martel, A.; Keane, M.; Tragger, C.; Basri, G. Night-Sky High-Resolution Spectral Atlas of OH and O Emission Lines for Echelle Spectrograph Wavelength Calibration. *Chic. J.* **1996**, *108*, 277–308. [CrossRef]
33. Rousselot, P.; Lidman, C.; Cuby, J.G.; Moreels, G.; Monnet, G. Night-sky spectral atlas of OH emission lines in the NIR. *Astron. Astrophys.* **1999**, *354*, 1134–1150.
34. French, W.J.R.; Burns, G.B.; Finlayson, K.; Greet, P.A.; Lowe, P.R.; Williams, P.F.B. Hydroxyl (6-2) airglow emission intensity ratios for rotational temperature determination. *Annu. Geophys.* **2000**, *18*, 1293–1303.
35. French, W.J.R.; Mulligan, F.J. Stability of temperatures from TIMED/SABER v1.07 (2002–2009) and Aura/MLS v2.2 (2004–2009) compared with OH(6-2) temperatures observed at Davis Station, Antarctica. *Atmos. Chem. Phys.* **2010**, *10*, 11439–11446. [CrossRef]
36. Dodd, J.A.; Blumberg, W.A.M.; Lipson, S.J.; Lowell, J.R.; Armstrong, P.S.; Smith, D.R.; Nadile, R.M.; Wheeler, N.B.; Huppi, E.R. OH(v,N) Column Densities from High-Resolution Earthlimb Spectra. *Geophys. Res. Lett.* **1993**, *20*, 305–308. [CrossRef]